



OPEN ACCESS

EDITED BY

Ahmed Makradi,
Luxembourg Institute of Science and
Technology (LIST), Luxembourg

REVIEWED BY

Julian David Correa,
Universidad de Medellín, Colombia
Jihyun Kim,
Seoul National University, South Korea

*CORRESPONDENCE

Jonghoon Lee,
✉ jonghoon.lee.1.ctr@afrl.af.mil
Ajit K. Roy,
✉ Ajit.Roy@afrl.af.mil

SPECIALTY SECTION

This article was submitted to Carbon-
Based Heterostructures,
a section of the journal
Frontiers in Carbon

RECEIVED 04 November 2022

ACCEPTED 02 December 2022

PUBLISHED 09 January 2023

CITATION

Lee J, Kedziora G, Glavin N and Roy AK
(2023), Counter charge cluster formation
in molecular doping of
molybdenum disulfide.
Front. Carbon 1:1089955.
doi: 10.3389/frcrb.2022.1089955

COPYRIGHT

© 2023 Lee, Kedziora, Glavin and Roy. This
is an open-access article distributed under
the terms of the [Creative Commons
Attribution License \(CC BY\)](#). The use,
distribution or reproduction in other
forums is permitted, provided the original
author(s) and the copyright owner(s) are
credited and that the original publication in
this journal is cited, in accordance with
accepted academic practice. No use,
distribution or reproduction is permitted
which does not comply with these terms.

Counter charge cluster formation in molecular doping of molybdenum disulfide

Jonghoon Lee^{1,2*}, Gary Kedziora¹, Nicholas Glavin¹ and Ajit K. Roy^{1*}

¹Materials and Manufacturing Directorate, Air Force Research Laboratory, Wright-Patterson Air Force Base, Dayton, OH, United States, ²ARCTOS Technology Solutions, Dayton, OH, United States

Studies of molybdenum disulfide (MoS₂) gas sensor prototypes report orders of magnitude higher sensitivity toward nitrogen dioxide (NO₂) over ammonia (NH₃). Based on the cluster formation model and density functional theory calculations of charge transfer, NO₂ was found to form a tightly bound cluster of counter charges upon carrier donation. In contrast, NH₃ forms only a semi-localized cluster of counter charges over a wide area of MoS₂, creating a larger collision cross section of coulomb interaction between the charge carrier and the counter charges. We discuss the potential effect of counter charge cluster localization on the efficiency of molecular doping.

KEYWORDS

gas sensor, molybdenum disulfide, molecular doping, density functional theory, charge transfer, counter charge cluster

1 Introduction

Ever since the prospect of single gas molecule detection was first discussed with a graphene device (Schedin et al., 2007), whose high sensitivity was partially attributed to the surface nature of graphene exposing its whole volume to the gas molecule adsorbates, a gamut of 2D materials have been examined for gas sensor applications. In particular, transition metal dichalcogenides (TMDCs) have proven to be among the best materials for 2D gas sensor applications because of their tunable electronic properties and high sensitivity at room temperature (He et al., 2012; Late et al., 2014; Ko et al., 2016; Shokri and Salami, 2016; Yang et al., 2017; Pandey et al., 2020). When exposed to the target gas, a TMDC gas sensor responds to the adsorption of target gas molecules by changing its electrical conductivity. Based on the results of Hall measurements (Schedin et al., 2007), photoluminescence (PL) spectroscopy (Mouri et al., 2013; Cho et al., 2015a; Wang et al., 2019), and theoretical considerations (Leenaerts et al., 2008; Wehling et al., 2008), the molecular gas adsorption was recognized as inducing charge transfer on TMDC and modulating the charge carrier density on the 2D device. Depending on whether the electrical conductivity of the 2D sensor was increasing or decreasing, the target gas molecule would be categorized as carrier-donating or -compensating.

Experimental studies of TMDC gas sensor devices often compare the sensitivity of the device to various kinds of gas molecules, where the sensitivity is defined as the change in electrical resistance upon gas sensing, normalized to the default resistance of the device in dry air (Cho et al., 2015a; Cho et al., 2015b; Hau et al., 2021). The dry air normalization is specifically used to reduce the amount of chemical doping from redox reactions involving water vapor. The reported sensitivity involves a significant degree of reversibility correlated with the partial pressure of the target gas molecules in the gas environment. This reversibility indicates that a corresponding amount of carrier doping is induced by the physisorption of gas molecules that readily desorb upon a decrease in the partial pressure of the target gas molecules in the air.

The most frequently targeted gas molecules in TMDC gas sensor studies are nitrogen dioxide (NO₂) and ammonia (NH₃) as they are the representative *p*-type and *n*-type molecular dopants. It has consistently been reported in the experimental literature that the sensitivity of TMDC gas sensors toward NO₂ is an order of magnitude higher than for NH₃, which holds true for both *n*-type and *p*-type TMDC devices (Cho et al., 2015a, Cho et al., 2015b; Hau et al., 2021). This means that the charge carrier density in the TMDC gas sensor is much more strongly affected by the presence of NO₂ than NH₃ in the gas environment under the same partial pressure. From this, it may be concluded that NO₂ should be a dopant with a superior efficiency compared to NH₃ and other gas molecules. However, the concept of doping efficiency as used previously is rather vague because correlating the experimentally measurable sensitivity with the partial pressure of target gas molecule in the environment involves multiple processes such as molecular adsorption and charge-state transition. In the following section, we discuss the processes involved in molecular doping and introduce counter charge cluster localization, which has been seldom mentioned in the literature, despite the fact that it can potentially affect doping efficiency.

The first event that must occur in the sensing process is the adsorption of gas molecules onto the exposed TMDC surface. The adsorption energy is the thermodynamic observable estimating the surface density of target gas molecules at equilibrium. Gas molecules with lower adsorption energy would have a greater chance of affecting the electronic properties of TMDC if the number of carriers donated or compensated positively correlated with the surface density of the gas molecules. Theoretical studies of gas molecule physisorption, however, found only nonsignificant differences (less than 10 meV) in the adsorption energies of NO₂ and NH₃ on TMDC (Yue et al., 2013). Therefore, the adsorption energy alone cannot be the main cause of the large differences in sensitivity of a TMDC sensor toward NO₂ and NH₃.

In analyzing doping efficiency, we need to measure more than the surface coverage of molecular adsorbates because not all the adsorbates are activated as dopants. The dopant activation process after adsorption results in charge transfer, for which there exist multiple plausible scenarios. The so-called chemical doping occurs especially at chemically heterogeneous reactive sites of structural defects and edges of TMDC. Integer charge transfer results from redox reactions involving not only the target gas molecule and TMDC but also ambient molecules of nitrogen, oxygen, and water (Li et al., 2017; Zhao et al., 2018). Such redox reactions are strongly dependent on ambient temperature and result in charge distribution near defects and edges, producing regions of carrier depletion and double-layer potential (Gautam et al., 2021). The other viable scenario of charge transfer involves physisorption of gas molecules, which is of our interest in this report. In this case, the so-called standard model of molecular doping examines the energies of the highest occupied molecular orbital (HOMO) and the lowest unoccupied molecular orbital (LUMO) of gas molecules relative to the Fermi level or work function of the hosting TMDC (Peng and Cho, 2000; Wehling et al., 2008; Park et al., 2019). If the LUMO of the gas molecules is lower than the Fermi level of hosting TMDC, the molecular gas adsorbate accepts electrons from TMDC. If the HOMO is higher than the Fermi level, the gas molecules become donors of electrons to TMDC. In essence, this model follows the Schottky–Mott rule of interface band bending, which interprets electron transfer as a transport phenomenon allowing two distinct

bodies of electron distribution in contact to reach equilibrium (Zhang and Yates, 2012). As this charge transfer process involves the Fermi level as an electron reservoir, the efficiency of gas molecular doping becomes a function of the Fermi level.

For conventional inorganic semiconductors where the conduction is predominantly band conduction *via* delocalized conduction band or the valence band, thermodynamic stability analyses of dopants at various charge states are routinely performed to address the efficiency of the dopant, such as whether it is a shallow or deep donor (Van de Walle and Neugebauer, 2004; Freysoldt et al., 2014; Alkauskas et al., 2016). However, the charged dopant stability analysis is not as frequently utilized for molecular doping of 2D materials, partly because our understanding of the conduction mechanism in TMDC gas sensors is still developing. It should be noted that electrons or holes transferred to the Fermi level of TMDC are not necessarily free-charge carriers if the Fermi level exists within the localized gap states. When the transferred charges are near the Fermi level but away from delocalized bands, they still conduct electricity *via* ‘hopping’ conduction (Shklovskii and Efros, 1984). In fact, this variable range hopping was reported as the governing conduction mechanism of TMDC thin films when the temperature was lower than room temperature (Qiu et al., 2013; Xue et al., 2019). Even near room temperature, the variable range hopping remained as the major channel of conduction in various 2D material thin films (Negishi et al., 2014; Kovtun et al., 2021). Considering the semi-crystalline quality of TMDC materials often adopted for gas sensor applications and research, it is plausible to assume that electrical conduction occurs through the multi-channel type of band conduction and hopping conduction, where the hopping conduction channel is rather predominant.

As outlined so far, the molecular doping of charge carriers and conduction in 2D material thin films are multifaceted phenomena. The outstanding experimental challenge preventing quantitative analysis lies in identifying the several physically distinguishable mechanisms simultaneously participating in charge transfer. Nevertheless, we can attest phenomenologically that the charge transfer between the gas molecular adsorbate and the hosting 2D material results in involves charge carriers conducting electricity along with the counter charges of the donated carriers localized upon the gas molecular adsorbate. As it is localized, the counter charge left on the adsorbate does not participate in the conduction. If anything, it would more likely hamper the mobility of the free carriers through coulomb scattering. Coulomb interactions between the free carrier and localized counter charges will affect the separation and recombination between them as well. However, as the subject of counter charge distribution has rarely been studied for molecular dopants, our understanding of how this would affect the efficiency of carrier doping is limited. As a side note, for polymer semiconductors, the effect of counter-ion size on delocalization of carriers was studied, although the subject was not the distribution of counter charges but the physical size of the counter-ions (Thomas et al., 2020).

The counter charge distribution upon charge carrier donation was first studied for conventional inorganic semiconductors, providing valuable insights toward overall understanding of carrier donation with unexpected findings (Schwingenschlögl et al., 2010). For carrier doping of conventional semiconductors of silicon and diamond, group III and group IV elements often substitute the host element to compensate or donate electrons. From the theoretical analysis of counter charge distribution upon carrier doping, it was found that the carrier donation was not executed solely by the dopant element but by the cluster of atoms composed of the dopant and nearby host atoms (Schwingenschlögl et al., 2010; 2011; Smith et al., 2017).

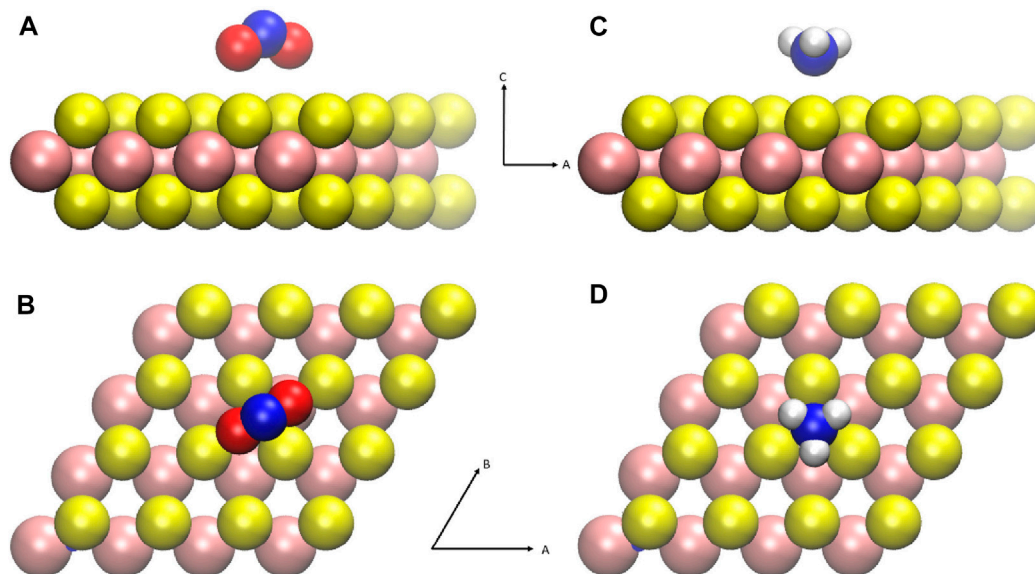


FIGURE 1

Schematic representation of gas molecules physisorbed on MoS₂. The size of the MoS₂ supercell is $4a \times 4a$, where a is the lattice constant of the MoS₂ primary unit cell, 3.197Å. The atomic configuration depicted here shows the lowest energy configuration calculated (Yue et al., 2013; Zhao et al., 2014; Cho et al., 2015a). (A,B) Side and top views of nitrogen dioxide physisorption configuration. (C,D) Side and top views of ammonia physisorption configuration. Colors refer to the following: Mo (pink), S (yellow), N (blue), O (red), and H (white).

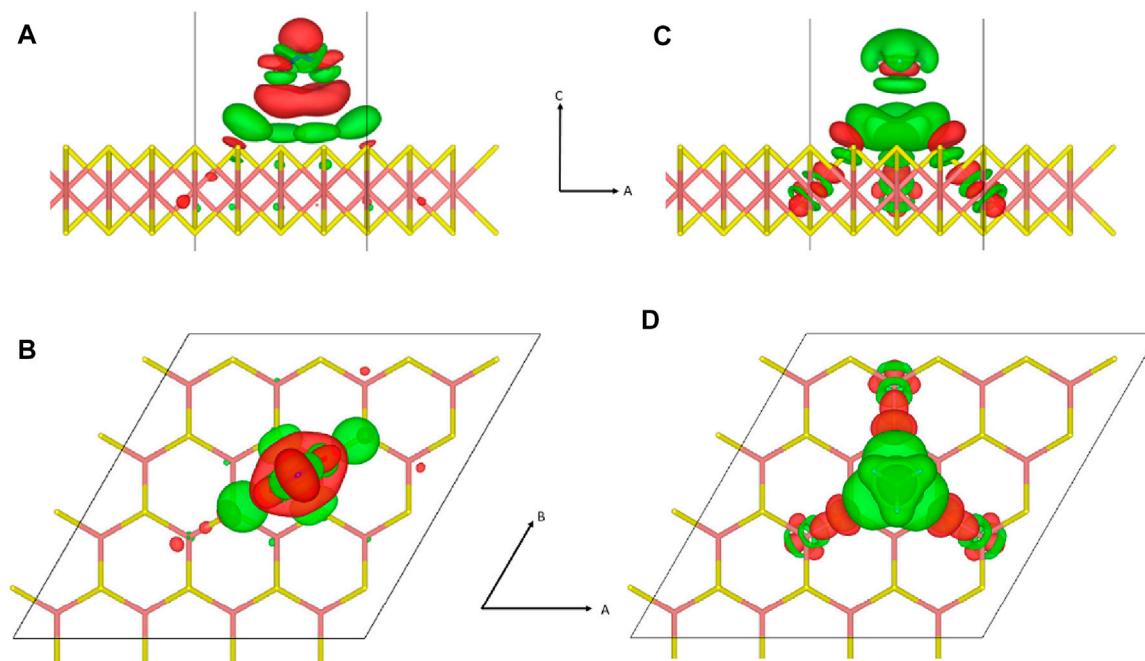


FIGURE 2

Redistribution of electrons upon physisorption of gas molecules is depicted with a density isosurface. Subfigure arrangement and atomic configurations are identical to those of Figure 1. (A,B) For NO₂ adsorption, the electron density isosurface at $\Delta\rho(\vec{r}) = \pm 0.46 \text{ e}/\text{\AA}^3$ is drawn in green (–) and red (+). A fractional charge of .04 (9)e was transferred from MoS₂ to NO₂ based on Bader charge analysis. (C,D) For NH₃ adsorption, the electron density isosurface at $\Delta\rho(\vec{r}) = \pm 0.69 \text{ e}/\text{\AA}^3$ is drawn in green (–) and red (+). A fractional charge of .04 (6)e was transferred from NH₃ to MoS₂ based on Bader charge analysis. The color scheme of sticks is as follows: Mo (pink), S (yellow), N (blue), O (red), and H (white).

The additional physical understanding provided by the cluster formation model distinguishes two different types of charge transfer associated with dopant–host interaction. For the example of silicon

doping using arsenic, as we look into the charge distribution between arsenic atoms and nearby silicon atoms, the electron distribution is shifted away from silicon toward arsenic because arsenic has stronger

electronegativity than silicon. However, in terms of carrier doping properties, arsenic is an *n*-type dopant donating an electron to the silicon lattice, which contradicts the direction of charge transfer based on strength of electronegativity. The cluster formation model of carrier doping resolved this apparent inconsistency, when it was found that the electron carrier was donated to the silicon lattice not by the arsenic atom alone but by a cluster of atoms including arsenic and nearby silicon atoms. Therefore, we note two distinguishable and uncorrelated charge transfers: a local charge transfer within a cluster with electrons shifting toward arsenic from silicon and a charge transfer as carrier doping between the arsenic cluster and the silicon lattice, wherein an electron moves from the arsenic cluster to the silicon lattice.

In this paper, we describe the nature of the charge transfer between a gas molecular adsorbate and 2D TMDC material based on the counter charge cluster formation model and density functional theory. Our system of interest is 2D molybdenum disulfide (MoS₂) as the archetypal TMDC along with ammonia (-NH₃) and nitrogen dioxide (-NO₂) as the representative molecular dopants of opposing doping property. As we addressed the differences between NO₂ and NH₃ as molecular dopants, we directed our attention not to the donated charge carrier but rather to the counter charges left localized on the molecular dopant. Unlike the donated charge carrier whose spatio-temporal property keeps varying as it transports, the counter charge distribution left on the molecular dopant would be essentially constant, as long as other charge carriers were not nearby. As discussed in the following sections, the counter charge cluster formation analysis upon carrier doping by molecular dopants allowed us to determine the drastically different activities of NO₂ and NH₃. NO₂ molecular adsorbates, upon donation of a hole, form a tightly localized cluster of counter charges centered around a NO₂ molecule. On the contrary, the counter charge cluster formed by NH₃ upon electron donation is only semi-localized and exhibits a dimension that is not well defined. The implication of such a qualitative difference on the doping efficiency is conjectured and discussed.

2 Materials and methods

To investigate the charge distribution in the gas molecular adsorbate complex, we used the Vienna *ab initio* simulation package (VASP) for the density functional theory (DFT) calculations (Hafner, 2008). Along with the exchange-correlation kernel of Perdew–Burke–Ernzerhof revised for solids (PBEsol), the projector augmented wave (PAW) pseudo-potentials for molybdenum (Mo) and sulfur (S) were adopted (Blöchl, 1994; Csonka et al., 2009). In this context, the electronic band gap energy of MoS₂ as the difference between the valence band maximum (VBM) and the conduction band minimum (CBM) in the ground state band structure was calculated to be 1.28 eV for the bilayer with a separation distance of 6.14 Å. Additional Bader charge analysis was also performed to attribute the electron distribution to each atomic and molecular entity (Tang et al., 2009). As Bader charge analysis utilizes the gradient of charge distribution, which is grid-based in VASP, a high-resolution grid between elements is necessary in charge-density calculations to reduce errors in Bader analyses. For the high-resolution grid, VASP calculations were performed with the ‘Accurate’ setting for PREC and the energy cutoff set to 420 eV, which is 1.5 times the

energy cutoff used for the molybdenum pseudo-potential, to convert the charge density on gas molecules with significant figures down to two decimal places of fundamental charge.

Figure 1 shows the ground state configurations of gas molecular physisorption widely studied and reported for MoS₂ gas sensing devices. The NO₂ and NH₃ molecules are characterized as hole donors and electron donors, respectively. Such gas molecular adsorbates affect the trion peaks of photoluminescence (Tongay et al., 2013; Cho et al., 2015a), indicating variations in the carrier density. The configurations shown in Figure 1 were used to calculate the charge distribution. For charged systems, the periodic image charge interaction should affect the charge cluster confinement. Therefore, four different values of the supercell lattice constant (*L*) were used to address the system size dependency of charge distribution, as with *L* = 4*a*, 8*a*, 12*a*, 16*a* where *a* = 3.20 Å is the lattice constant of the MoS₂ unit cell.

The charge distribution was calculated before and after carrier donation (Schwingenschlöggl et al., 2010; 2011; Smith et al., 2017). The charge transfer before carrier donation occurred locally in the dopant complex, a region of adsorbate and nearby host elements. A weak hybridization between nearby molecular orbitals rearranges the electron distribution resulting in shifting of charges. The magnitude of such charge transfer is only fractional, however. More importantly, it does not contribute to electrical conduction because transferred charges are localized at the adsorbate complex. The charge state of the overall system remains neutral because no charge leaves the adsorbate and its surroundings. On the contrary, when charge transfer happens between the adsorbate complex and the electron reservoir of the system’s Fermi level, as in carrier donation, the adsorbate complex becomes counter charged. By analyzing the distribution of this counter charge in the adsorbate complex, we investigated the formation of the counter charge cluster.

It should be noted that our interest is in charge distribution only, not on the free energy of the charged system. Addressing free energy of the various charge states of a dopant system often assumes a single isolated dopant in an infinite host, which requires corrections of various supercell artifacts (Van de Walle and Neugebauer, 2004; Persson et al., 2005; Lany and Zunger, 2008; Freysoldt et al., 2009; 2014; Alkauskas et al., 2016). For 2D charged systems of slab and surfaces, the methodological consensus is still being sought after regarding the correction of even stronger coulomb self-interactions through a vacuum (Komsa and Pasquarello, 2013; Komsa et al., 2014; Freysoldt and Neugebauer, 2018; O’Hara et al., 2019; Rutter, 2021).

3 Results with discussion

As outlined in the Introduction section, the molecular doping *via* gas molecular physisorption goes through processes of adsorption and charge-state transition. Adsorption is a local event, while the transition in the charge state of the adsorbate is a process depending on the Fermi level of the host. Each process is accompanied by charge transfers with different characteristics and magnitudes, which are discussed separately in the following sections.

3.1 Adsorbate complex formation

First, we discuss the local charge transfer upon adsorption. As gas molecules approach the MoS₂ substrate, weak hybridizations between

molecular orbitals result in redistribution of electrons among the elements belonging to the physisorbed gas molecules and the substrate atoms near the adsorption site, satisfying the difference in electron affinity among elements involved in the specific adsorbate configuration. Quantitatively, the redistribution in electron density ($\Delta\rho$) upon adsorption can be expressed as follows:

$$\Delta\rho(\vec{r}) = \rho(\vec{r}; \text{MoS}_2 + \text{mole}) - \{\rho(\vec{r}; \text{MoS}_2) + \rho(\vec{r}; \text{mole})\}, \quad (1)$$

where $\rho(\vec{r}; \text{MoS}_2 + \text{mole})$ is the electron density at position \vec{r} after adsorption, while $\rho(\text{MoS}_2)$ and $\rho(\text{mole})$ are electron densities of the MoS₂ substrate and the gas molecules (mole) when widely separated. The charge transfer during this adsorption process is a redistribution within the system without any charge leaving or entering the system. Therefore, the overall charge state of the adsorbate system is neutral: $\int d\vec{r}\Delta\rho = 0$. Figure 2 shows such a redistribution with charge density iso-surfaces for the adsorption of NO₂ and NH₃.

Applying Bader charge analysis to $\Delta\rho(\vec{r})$, we identified the amount of charge transfer between the gas molecular adsorbate and the substrate atoms near the adsorption site. In our calculations, roughly 5% of the fundamental charge is shifted toward NO₂ from the substrate, while a similar amount of charge is shifted away from NH₃ toward the substrate. Although the amount of shifted charge may vary slightly depending on the level of theory and the charge analysis method adopted in DFT calculations, the magnitude is only fractional and minuscule in other reports as well (Leenaerts et al., 2008; Yue et al., 2013). What should be noted is that the fractional charge, either positive or negative, shifted to the adsorbent is spatially localized and confined to the region proximate to the adsorbate, rendering a small yet finite charge dipole or polarization in the region around the adsorbate.

More often than not, the direction of this polarization is qualitatively associated with the experimental categorization as to whether the gas molecule is an electron donor or an acceptor (Yue et al., 2013; Wang et al., 2019). However, this is only coincidental and situational because of the following reasons. First, the transferred charge is not free to be conducted because it is spatially localized near the molecular adsorbate. Second, the amount of charge transferred is fractional, representing only a few percent of the elemental charge, while the photoluminescence spectroscopy data are consistent with integer charge carrier doping with a trion peak (Cho et al., 2015a). Such minuscule amounts of fractional charge are thought to accumulate into integer charges when combined from an ensemble of dopants (Tongay et al., 2013). However, such arguments could be realized only if the transferred charge resides in the delocalized band or metal where charges are free to move and gather. Third, the direction of polarization depends on the adsorbate configuration, which contradicts the standard doping model where the doping property is independent of the adsorbate configuration (Leenaerts et al., 2008). Fourth, this hypothesis assumes that the carrier donation should happen between the gas molecule and the nearby adsorbent atoms. As observed in the counter charge cluster formation model, it is not the donor alone but a cluster of atoms including the donor and nearby host atoms that donates the carrier (Schwingenschlögl et al., 2010; 2011).

In the charge transfer depicted in Figure 2, the charge state of the whole system remains neutral because there is no change in the total number of electrons in the system. Actually, what we observe from the charge redistribution in Figure 2 is the formation of an adsorbate complex encompassing the adsorbate molecule and proximate

adsorbent atoms affected by the adsorbate, which has little to do with charge carrier doping. As we refer to an analogical charge transfer, which is both *fractional* and *local*, a similar dopant complex formation can be identified in conventional silicon doping despite the difference in chemical bonding. When a group III or IV dopant atom substitutes for a silicon atom in the silicon lattice, the dopant atom forms multiple covalent bonds with nearby silicon atoms. Due to differences in the electronegativity between silicon atoms and the dopant atom, the covalent bonds of the silicon–dopant pair become polar with a fractional shifting of charges. However, this fractional rearrangement of charge distribution near the dopant atom has nothing to do with carrier doping resulting from the charge transfer between the dopant complex and the delocalized conduction or valence band of the lattice. For example, although both boron and gallium are *p*-type dopants in a silicon lattice, the polarity in the polar-covalent bonds in the boron–silicon pair and the gallium–silicon pair are opposite to each other because boron is more electronegative than silicon, while gallium is less electronegative than silicon (Schwingenschlögl et al., 2010). The direction of polarity in the polar-covalent bond involving a dopant atom may agree or disagree with the actual doping property of the dopant, which is only coincidental.

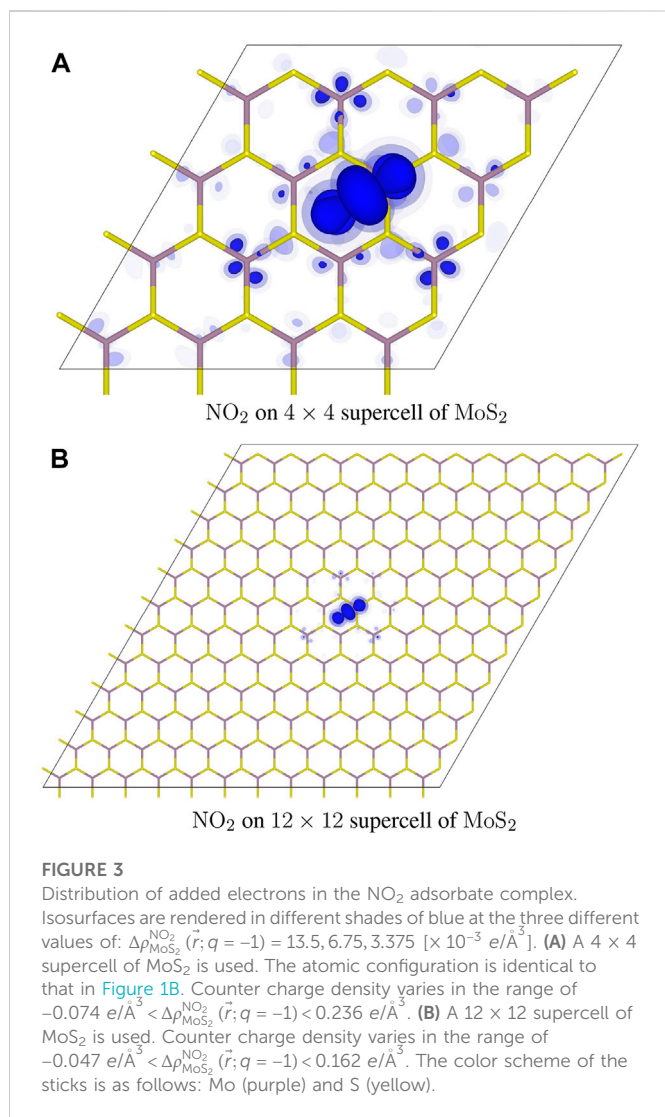
3.2 Counter charge cluster formation

The standard molecular doping model describes the energetically favored charge transfers between HOMO (or LUMO) of the molecular adsorbate dopant and the Fermi level of the hosting material as electron reservoir (Peng and Cho, 2000; Wehling et al., 2008; Park et al., 2019). The charge carrier, whether it is an electron or a hole donated by the molecular adsorbate to the hosting material, should participate in the electrical conduction in the host, while the counter charge of the carrier remains on the adsorbate dopant. Assuming charge transfer between the dopant and the Fermi level of the host (Schwingenschlögl et al., 2010; 2011; Smith et al., 2017), we calculated the distribution of counter charges in the supercell of MoS₂ with molecular adsorbate. The counter charge distribution indicates the domain of the cluster from which the charge carrier is donated.

If the Fermi level of the system is near the delocalized conduction or valence band of MoS₂, the charge transfer between the molecular adsorbate and the Fermi level will donate free carriers for band conduction in the hosting lattice. However, as hopping conduction is often reported as the major conduction mechanism in 2D TMDC thin films (Qiu et al., 2013; Xue et al., 2019; Kovtun et al., 2021), we assumed that charge transfer happened between the molecular adsorbate and other defect sites near the Fermi level. The transferred charge would conduct electricity through hopping along the percolated path of defect sites (Shklovskii and Efros, 1984). To address the counter charge distribution on the molecular adsorbate after carrier doping, we subtracted the electron density of the adsorbate system (MoS₂+mole) in the neutral charge state $\rho_{\text{MoS}_2}^{\text{mole}}(\vec{r}; q = 0)$ from the electron density of the same system in the counter-charged state: $\rho_{\text{MoS}_2}^{\text{mole}}(\vec{r}; q = q')$, where q' is the counter charge of the donated carrier in units of elemental charge localized on the adsorbate:

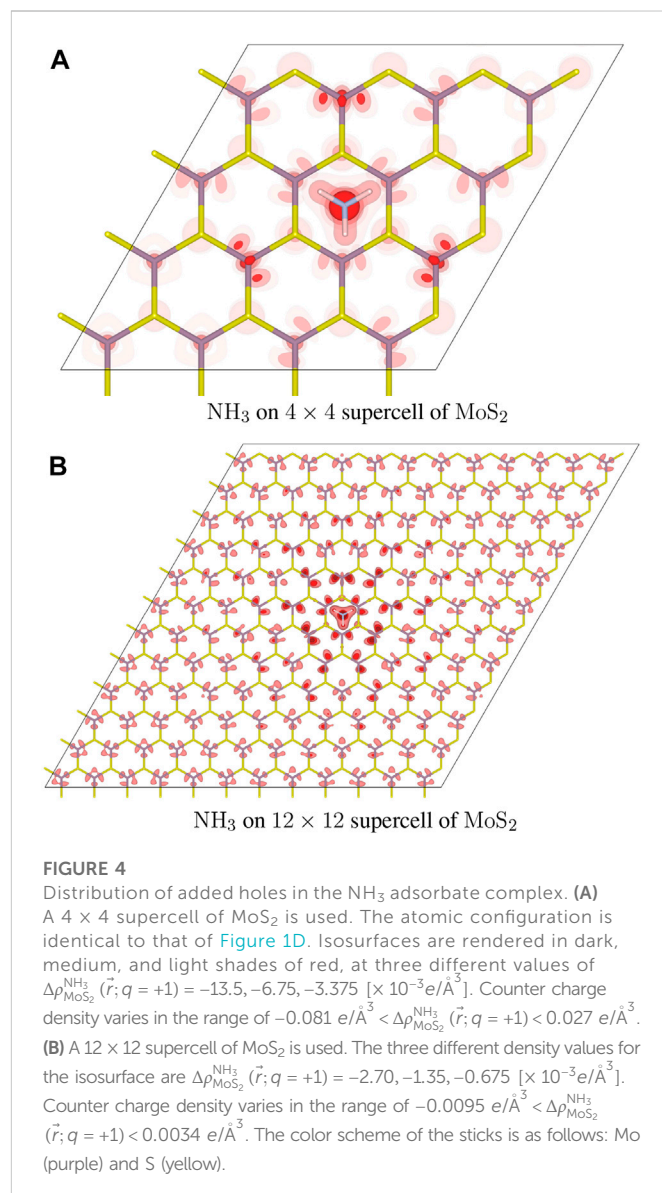
$$\Delta\rho_{\text{MoS}_2}^{\text{mole}}(\vec{r}; q = q') = \rho_{\text{MoS}_2}^{\text{mole}}(\vec{r}; q = q') - \rho_{\text{MoS}_2}^{\text{mole}}(\vec{r}; q = 0). \quad (2)$$

For the *p*-type dopant of the NO₂ molecular adsorbate, Figure 3 shows the counter charge distribution, $\Delta\rho_{\text{MoS}_2}^{\text{NO}_2}(\vec{r}; q = -1)$. The



added electron is distributed over a tightly bound cluster composed of NO₂ and nearby host atoms of MoS₂. It should be noted that the cluster is well centered on NO₂ as its shape depends little on changes in the MoS₂ supercell dimensions. Figure 5A shows that the characteristic size of the counter charge cluster is well defined as the counter charge density in MoS₂ shows an exponential decay with distance from NO₂.

The *n*-type doping of NH₃ involves an electron transfer from a cluster surrounding NH₃ to the Fermi level of MoS₂. Figure 4 shows the distribution of counter charge, $\Delta\rho_{\text{MoS}_2}^{\text{NH}_3}(\vec{r}; q = +1)$, from where the donated electron left the adsorbate. Although the counter charge distribution is centered on NH₃, it is not as strongly bounded as in the case of NO₂. Along with the increase in the lattice constant of the MoS₂ supercell, the spatial extent of the counter charge distribution also expands. Figure 5B shows the semi-localized nature of the counter charge cluster on NH₃. The counter charge density in MoS₂ is higher near NH₃ as it is localized, but then it slowly decreases with distance from the adsorption site. The distribution is a strong function of the system size without any characteristic length definable as it is delocalized. The maximum counter charge density decreases as the counter charge spreads out further with increasing system size.

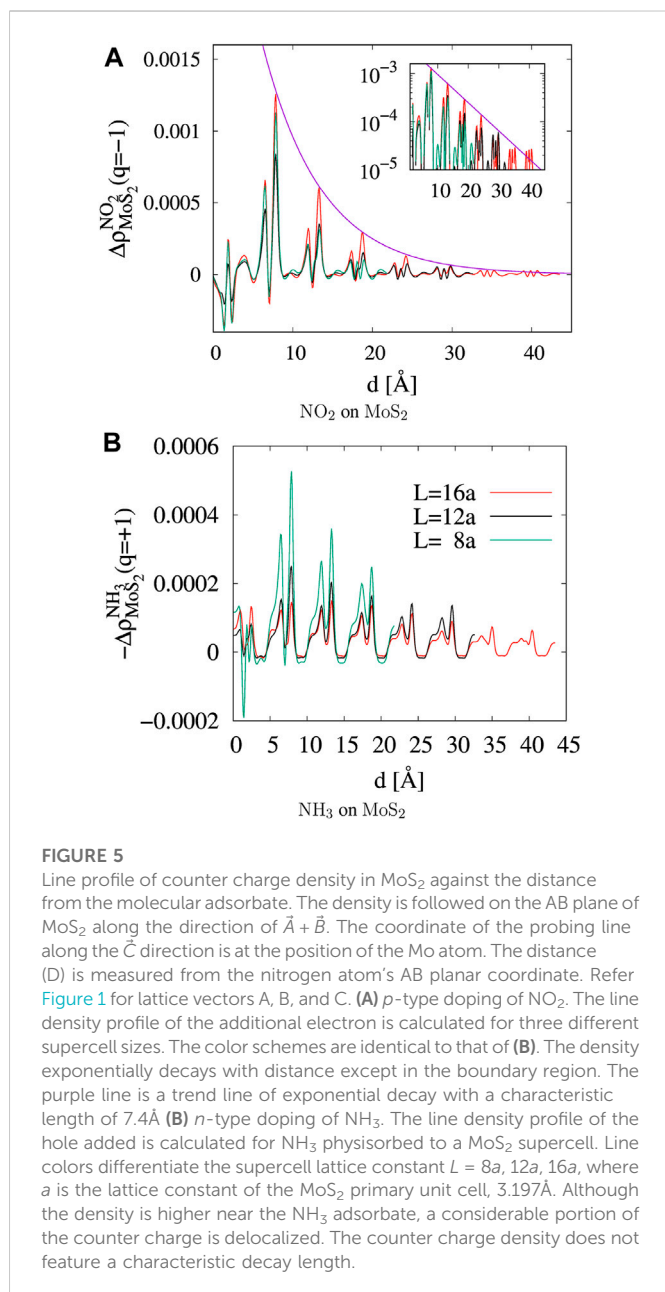


From Bader charge analysis, which specifies the amount of counter charge assumed by the gas molecule itself, we can estimate the Fukui index ($f_{+/-}$) of gas molecular adsorbates as follows:

$$f_+(\text{NO}_2) = Q_{\text{NO}_2}(N+1) - Q_{\text{NO}_2}(N), \quad (3)$$

$$f_-(\text{NH}_3) = Q_{\text{NH}_3}(N) - Q_{\text{NH}_3}(N-1), \quad (4)$$

where $Q_{\text{mole}}(N)$ is the charge on a gas molecule when N is the number of electrons in the system at neutral charge state. The Fukui index estimates the electrophilicity (f_+) of NO₂ and the nucleophilicity (f_-) of NH₃ when the system is charged with additional or a reduced number of electrons (Geerlings et al., 2003). Figure 6 and Table 1 show that the electrophilicity of the NO₂ molecule converges to around 0.25 with increasing system size, while the remaining 75% of electron is distributed over the MoS₂ atoms in the cluster. However, the NH₃ molecule shows a nucleophilicity that diminishes as the system size increases. The

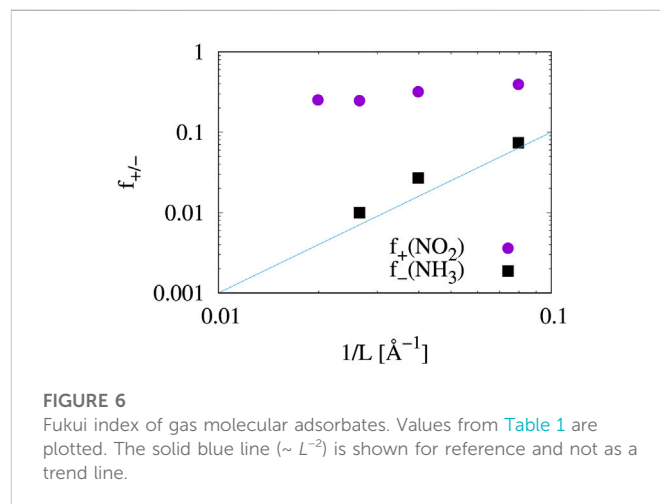


amount of counter charge residing on the NH₃ molecule becomes negligible for an isolated NH₃ adsorbate.

Although the subject of counter charge clusters is a rare topic in the literature of molecular doping, there are multiple scenarios of possible effects of counter charge distribution and localization on charge carriers. The electrostatic interaction between the carrier and its counter charge is central to the activation and transient recombination of the carrier. The interaction between counter charges is another subject deserving of attention as its screening would affect the surface density of the activated dopants. Not only the carrier density but also the mobility of the carrier depends on counter charge distribution; the spatial dimension and strength of localization of the counter charge clusters will generate the interaction potential landscape which the carrier has to navigate through. Considering the stronger 2D coulomb interaction rendering short exciton lifetimes of a few

TABLE 1 Fukui index of molecular adsorbates.

System size	Electrophilicity of NO ₂	Nucleophilicity of NH ₃
(L/a)	$f_+(\text{NO}_2)$	$f_-(\text{NH}_3)$
4	.39 (4)	.07 (4)
8	.31 (9)	.02 (7)
12	.24 (8)	.01 (0)
16	.25 (2)	-.00 (1)



nanoseconds (Palummo et al., 2015; H-L et al., 2020), the influence of counter charge distribution on the efficiency of carrier doping deserves greater attention from the research community.

NO₂ and NH₃ are gas molecules with opposite doping characteristics most frequently adopted in testing gas sensor application of layered MoS₂. Based on the counter charge cluster formation upon carrier donation, NO₂ fits the physical picture of the standard doping model quite well, rendering a spatially well confined cluster of counter charge localized on NO₂. In contrast, NH₃ forms only a semi-localized cluster of counter charge centered on the molecule. It is noteworthy that these two gas molecules with vast differences in doping efficiency feature counter charge clusters of qualitatively distinguishable characteristics.

4 Conclusion

Gas sensor devices based on two-dimensional layered transition metal dichalcogenides feature desirable properties such as high sensitivity and room temperature operation. The sensing mechanism is based on the change in charge carrier density upon gas molecular adsorption. MoS₂ gas sensors show an order of magnitude higher sensitivity toward NO₂ over NH₃ (Cho et al., 2015a; Hau et al., 2021). For the case of charge carrier doping from gas molecular physisorption, the counter charge cluster formation was investigated using density functional theory

calculations of charge density. The standard doping model assumes a delocalized charge carrier with a localized counter charge at the dopant, which accords well with the *p*-type dopant molecule, NO₂. A quarter of an elemental charge is physically distributed on the NO₂ molecule, while the remaining portion of the elemental charge is distributed over the hosting MoS₂ within the counter charge cluster.

The nature of the positive counter charge clusters formed by NH₃ upon electron donation is very different. Although the distribution of the counter charge is centered around the NH₃ adsorbate, the cluster is only semi-localized and does not have a definite size. The amount of actual counter charge possessed by NH₃ molecules is actually negligible as most of the counter charge is assumed by host atoms in the cluster. Although the effect of counter charge distribution on carrier dynamics and doping has not been systematically studied, it is conjectured that the wider distribution of semi-localized counter charge may hamper the sensitivity of gas sensors by reducing the carrier mobility through an enhanced scattering cross section and also by promoting transient recombination with the delocalized carriers.

Data availability statement

The original contributions presented in the study are included in the article/Supplementary Material; further inquiries can be directed to the corresponding authors.

References

- Alkauskas, A., McCluskey, M. D., and Van de Walle, C. G. (2016). Tutorial: Defects in semiconductors—combining experiment and theory. *J. Appl. Phys.* 119, 181101. doi:10.1063/1.4948245
- Blöchl, P. E. (1994). Projector augmented-wave method. *Phys. Rev. B* 50, 17953–17979. doi:10.1103/PhysRevB.50.17953
- Cho, B., Hahm, M. G., Choi, M., Yoon, J., Kim, A. R., Lee, Y.-J., et al. (2015a). Charge-transfer-based gas sensing using atomic-layer MoS₂. *Sci. Rep.* 5, 8052. doi:10.1038/srep08052
- Cho, B., Kim, A. R., Park, Y., Yoon, J., Lee, Y.-J., Lee, S., et al. (2015b). Bifunctional sensing characteristics of chemical vapor deposition synthesized atomic-layered MoS₂. *ACS Appl. Mater. Interfaces* 7, 2952–2959. doi:10.1021/am508535x
- Csonka, G. I., Perdew, J. P., Ruzsinszky, A., Philippen, P. H. T., Lebegue, S., Paier, J., et al. (2009). Assessing the performance of recent density functionals for bulk solids. *Phys. Rev. B* 79, 155107. doi:10.1103/PhysRevB.79.155107
- Freysoeldt, C., Grabowski, B., Hickel, T., Neugebauer, J., Kresse, G., Janotti, A., et al. (2014). First-principles calculations for point defects in solids. *Rev. Mod. Phys.* 86, 253–305. doi:10.1103/RevModPhys.86.253
- Freysoeldt, C., and Neugebauer, J. (2018). First-principles calculations for charged defects at surfaces, interfaces, and two-dimensional materials in the presence of electric fields. *Phys. Rev. B* 97, 205425. doi:10.1103/PhysRevB.97.205425
- Freysoeldt, C., Neugebauer, J., and Van de Walle, C. G. (2009). Fully ab initio finite-size corrections for charged-defect supercell calculations. *Phys. Rev. Lett.* 102, 016402. doi:10.1103/PhysRevLett.102.016402
- Gautam, Y. K., Sharma, K., Tyagi, S., Ambedkar, A. K., Chaudhary, M., and Pal Singh, B. (2021). Nanostructured metal oxide semiconductor-based sensors for greenhouse gas detection: Progress and challenges. *R. Soc. Open Sci.* 8, 201324. doi:10.1098/rsos.201324
- Geerlings, P., De Proft, F., and Langenaeker, W. (2003). Conceptual density functional theory. *Chem. Rev.* 103, 1793–1874. doi:10.1021/cr990029p
- H-L, P., Mondal, P., Bid, A., and Basu, J. K. (2020). Electrical and chemical tuning of exciton lifetime in monolayer MoS₂ for field-effect transistors. *ACS Appl. Nano Mater.* 3, 641–647. doi:10.1021/acsnm.9b02170
- Hafner, J. (2008). *Ab-initio* simulations of materials using VASP: Density-functional theory and beyond. *J. Comput. Chem.* 29, 2044–2078. doi:10.1002/jcc.21057
- Hau, H. H., Duong, T. T. H., Man, N. K., Thi Viet Nga, T., Thi Xuan, C., Thi Thanh Le, D., et al. (2021). Enhanced NO₂ gas-sensing performance at room temperature using exfoliated MoS₂ nanosheets. *Sensors Actuators A Phys.* 332, 113137. doi:10.1016/j.sna.2021.113137
- He, Q., Zeng, Z., Yin, Z., Li, H., Wu, S., Huang, X., et al. (2012). Fabrication of flexible MoS₂ thin-film transistor arrays for practical gas-sensing applications. *Small* 8, 2994–2999. doi:10.1002/smll.201201224
- Ko, K. Y., Song, J.-G., Kim, Y., Choi, T., Shin, S., Lee, C. W., et al. (2016). Improvement of gas-sensing performance of large-area tungsten disulfide nanosheets by surface functionalization. *ACS Nano* 10, 9287–9296. doi:10.1021/acsnano.6b03631
- Komsa, H.-P., Berseneva, N., Krashennnikov, A. V., and Nieminen, R. M. (2014). Charged point defects in the flatland: Accurate formation energy calculations in two-dimensional materials. *Phys. Rev. X* 4, 031044. doi:10.1103/PhysRevX.4.031044
- Komsa, H.-P., and Pasquarello, A. (2013). Finite-size supercell correction for charged defects at surfaces and interfaces. *Phys. Rev. Lett.* 110, 095505. doi:10.1103/PhysRevLett.110.095505
- Kovtun, A., Candini, A., Vianelli, A., Boschi, A., Dell'Elce, S., Gobbi, M., et al. (2021). Multiscale charge transport in van der Waals thin films: Reduced graphene oxide as a case study. *ACS Nano* 15, 2654–2667. doi:10.1021/acsnano.0c07771
- Lany, S., and Zunger, A. (2008). Assessment of correction methods for the band-gap problem and for finite-size effects in supercell defect calculations: Case studies for ZnO and GaAs. *Phys. Rev. B* 78, 235104. doi:10.1103/PhysRevB.78.235104
- Late, D. J., Doneux, T., and Bougouma, M. (2014). Single-layer MoSe₂ based NH₃ gas sensor. *Appl. Phys. Lett.* 105, 233103. doi:10.1063/1.4903358
- Leenaerts, O., Partoens, B., and Peeters, F. M. (2008). Adsorption of H₂O, NH₃, CO, NO₂, and NO on graphene: A first-principles study. *Phys. Rev. B* 77, 125416. doi:10.1103/PhysRevB.77.125416
- Li, X., Li, X., Li, Z., Wang, J., and Zhang, J. (2017). WS₂ nanoflakes based selective ammonia sensors at room temperature. *Sensors Actuators B Chem.* 240, 273–277. doi:10.1016/j.snb.2016.08.163
- Mouri, S., Miyauchi, Y., and Matsuda, K. (2013). Tunable photoluminescence of monolayer MoS₂ via chemical doping. *Nano Lett.* 13, 5944–5948. doi:10.1021/nl403036h
- Negishi, R., Akabori, M., Ito, T., Watanabe, Y., and Kobayashi, Y. (2016). Band-like transport in highly crystalline graphene films from defective graphene oxides. *Sci. Rep.* 6, 28936. doi:10.1038/srep28936
- O'Hara, A., Tuttle, B. R., Zhang, X.-G., and Pantelides, S. T. (2019). *Formation energies of charged defects in two-dimensional materials – resolution of long-standing difficulties.* doi:10.48550/ARXIV.1911.11192
- Palummo, M., Bernardi, M., and Grossman, J. C. (2015). Exciton radiative lifetimes in two-dimensional transition metal dichalcogenides. *Nano Lett.* 15, 2794–2800. doi:10.1021/nl503799t

Author contributions

JL, NG, and AR conceived the idea of this study. JL, GK, and AR designed this study. JL developed the draft of this manuscript. All authors discussed the results and contributed to the final manuscript.

Conflict of interest

Author JL was employed by the company ARCTOS Technology Solutions.

The remaining authors declare that the research was conducted in the absence of any commercial or financial relationships that could be construed as a potential conflict of interest.

The handling editor is currently organizing a research topic with the author, AR.

Publisher's note

All claims expressed in this article are solely those of the authors and do not necessarily represent those of their affiliated organizations, or those of the publisher, the editors, and the reviewers. Any product that may be evaluated in this article, or claim that may be made by its manufacturer, is not guaranteed or endorsed by the publisher.

- Pandey, S. K., Das, R., and Mahadevan, P. (2020). Layer-dependent electronic structure changes in transition metal dichalcogenides: The microscopic origin. *ACS Omega* 5, 15169–15176. doi:10.1021/acsomega.0c01138
- Park, S., Schultz, T., Xu, X., Wegner, B., Aljarb, A., Han, A., et al. (2019). Demonstration of the key substrate-dependent charge transfer mechanisms between monolayer mos2 and molecular dopants. *Commun. Phys.* 2, 109. doi:10.1038/s42005-019-0212-y
- Peng, S., and Cho, K. (2000). Chemical control of nanotube electronics. *Nanotechnology* 11, 57–60. doi:10.1088/0957-4484/11/2/303
- Persson, C., Zhao, Y.-J., Lany, S., and Zunger, A. (2005). *n*-type doping of CuInSe₂ and CuGaSe₂. *Phys. Rev. B* 72, 035211. doi:10.1103/PhysRevB.72.035211
- Qiu, H., Xu, T., Wang, Z., Ren, W., Nan, H., Ni, Z., et al. (2013). Hopping transport through defect-induced localized states in molybdenum disulphide. *Nat. Commun.* 4, 2642. doi:10.1038/ncomms3642
- Rutter, M. J. (2021). Charged surfaces and slabs in periodic boundary conditions. *Electron. Struct.* 3, 015002. doi:10.1088/2516-1075/abeda2
- Schedin, F., Geim, A. K., Morozov, S. V., Hill, E. W., Blake, P., Katsnelson, M. I., et al. (2007). Detection of individual gas molecules adsorbed on graphene. *Nat. Mater* 6, 652–655. doi:10.1038/nmat1967
- Schwingenschlögl, U., Chroneos, A., Schuster, C., and Grimes, R. W. (2011). Doping and cluster formation in diamond. *J. Appl. Phys.* 110, 056107. doi:10.1063/1.3633223
- Schwingenschlögl, U., Chroneos, A., Schuster, C., and Grimes, R. W. (2010). Extrinsic doping in silicon revisited. *Appl. Phys. Lett.* 96, 242107. doi:10.1063/1.3455313
- Shklovskii, B. I., and Efros, A. L. (1984). *Electronic properties of doped semiconductors*. Springer Berlin, Heidelberg.
- Shokri, A., and Salami, N. (2016). Gas sensor based on MoS₂ monolayer. *Sensors Actuators B Chem.* 236, 378–385. doi:10.1016/j.snb.2016.06.033
- Smith, J. S., Budi, A., Per, M. C., Vogt, N., Drumm, D. W., Hollenberg, L. C. L., et al. (2017). *Ab initio* calculation of energy levels for phosphorus donors in silicon. *Sci. Rep.* 7, 6010. doi:10.1038/s41598-017-06296-8
- Tang, W., Sanville, E., and Henkelman, G. (2009). A grid-based bader analysis algorithm without lattice bias. *J. Phys. Condens. Matter* 21, 084204. doi:10.1088/0953-8984/21/8/084204
- Thomas, E. M., Peterson, K. A., Balzer, A. H., Rawlings, D., Stingelin, N., Segalman, R. A., et al. (2020). Effects of counter-ion size on delocalization of carriers and stability of doped semiconducting polymers. *Adv. Electron. Mater.* 6, 2000595. doi:10.1002/aelm.202000595
- Tongay, S., Zhou, J., Ataca, C., Liu, J., Kang, J. S., Matthews, T. S., et al. (2013). Broad-range modulation of light emission in two-dimensional semiconductors by molecular physisorption gating. *Nano Lett.* 13, 2831–2836. doi:10.1021/nl4011172
- Van de Walle, C. G., and Neugebauer, J. (2004). First-principles calculations for defects and impurities: Applications to III-nitrides. *J. Appl. Phys.* 95, 3851–3879. doi:10.1063/1.1682673
- Wang, Y., Slassi, A., Stoeckel, M.-A., Bertolazzi, S., Cornil, J., Beljonne, D., et al. (2019). Doping of monolayer transition-metal dichalcogenides via physisorption of aromatic solvent molecules. *J. Phys. Chem. Lett.* 10, 540–547. doi:10.1021/acs.jpclett.8b03697
- Wehling, T. O., Novoselov, K. S., Morozov, S. V., Vdovin, E. E., Katsnelson, M. I., Geim, A. K., et al. (2008). Molecular doping of graphene. *Nano Lett.* 8, 173–177. doi:10.1021/nl072364w
- Xue, J., Huang, S., Wang, J. Y., and Xu, H. Q. (2019). Mott variable-range hopping transport in a mos2 nanoflake. *RSC Adv.* 9, 17885–17890. doi:10.1039/c9ra03150b
- Yang, S., Jiang, C., and Wei, S.-h. (2017). Gas sensing in 2D materials. *Appl. Phys. Rev.* 4, 021304. doi:10.1063/1.4983310
- Yue, Q., Shao, Z., Chang, S., and Li, J. (2013). Adsorption of gas molecules on monolayer MoS₂ and effect of applied electric field. *Nanoscale Res. Lett.* 8, 425. doi:10.1186/1556-276X-8-425
- Zhang, Z., and Yates, J. T. (2012). Band bending in semiconductors: Chemical and physical consequences at surfaces and interfaces. *Chem. Rev.* 112, 5520–5551. doi:10.1021/cr3000626
- Zhao, S., Li, Z., Wang, G., Liao, J., Lv, S., and Zhu, Z. (2018). Highly enhanced response of MoS₂/porous silicon nanowire heterojunctions to NO₂ at room temperature. *RSC Adv.* 8, 11070–11077. doi:10.1039/C7RA13484C
- Zhao, S., Xue, J., and Kang, W. (2014). Gas adsorption on MoS₂ monolayer from first-principles calculations. *Chem. Phys. Lett.* 595–596, 35–42. doi:10.1016/j.cplett.2014.01.043